PERSPECTIVE

Check for updates

The necessity of periodic boundary conditions for the accurate calculation of crystalline terahertz spectra†

Peter A. Banks, [ID] Luke Burgess and Michael T. Ruggiero [ID]*

Terahertz vibrational spectroscopy has emerged as a powerful spectroscopic technique, providing valuable information regarding long-range interactions – and associated collective dynamics – occurring in solids. However, the terahertz sciences are relatively nascent, and there have been significant advances over the last several decades that have profoundly influenced the interpretation and assignment of experimental terahertz spectra. Specifically, because there do not exist any functional group or material-specific terahertz transitions, it is not possible to interpret experimental spectra without additional analysis, specifically, computational simulations. Over the years simulations utilizing periodic boundary conditions have proven to be most successful for reproducing experimental terahertz dynamics, due to the ability of the calculations to accurately take long-range forces into account. On the other hand, there are numerous reports in the literature that utilize gas phase cluster geometries, to varying levels of apparent success. This perspective will provide a concise introduction into the terahertz sciences, specifically terahertz spectroscopy, followed by an evaluation of gas phase and periodic simulations for the assignment of crystalline terahertz spectra, highlighting potential pitfalls and good practice for future endeavors.

1 Introduction

Terahertz vibrational spectroscopy is a powerful technique for studying intermolecular interactions in the condensed phase, having been demonstrated to be useful for a wide-array of applications.[1–6] At terahertz frequencies (0.1–10 THz or 3–333 cm^{-1}) large-amplitude complex motions of entire molecules are excited and sampled, and thus terahertz spectroscopy is a highly-sensitive probe of weak, often non-covalent, forces. The unique combination of sampling weak forces while probing long-range collective dynamics has spurred the growth of two, often related, lines of study. In the case of the former, weak forces in the condensed phase are inextricably dictated by the bulk packing of the individual molecules, making terahertz methods highly-sensitive to variations in three-dimensional structures. This has made terahertz spectroscopy a powerful complement to traditional structural methods (*e.g.*, X-ray diffraction) for the identification of different packing geometries, as observed in crystalline polymorphs, for example.[7–10] On the

Department of Chemistry, University of Vermont, 82 University Place, Burlington, Vermont 05405, USA. E-mail: michael.ruggiero@uvm.edu

† Electronic supplementary information (ESI) available: All molecular geometries and predicted frequencies. Animations of discussed vibrational modes. See DOI: 10.1039/d1cp02496e

other hand, the complex and large-amplitude motions occurring at terahertz frequencies have recently been related to a wide-variety of bulk phenomena, for example phase transformations,[11,12] mechanical responses,[5,13,14] electron–phonon coupling,[15,16] and gas-capture in porous materials.[17,18]

Unfortunately, the factors that make terahertz spectroscopy a valuable analytical technique simultaneously lead to one of its biggest challenges – the interpretation of experimental results. Unlike mid-infrared (mid-IR) methods, such as Fourier transform infrared spectroscopy (FTIR) and mid-IR Raman scattering, there do not exist any functional-group specific transitions at terahertz frequencies. Each individual bulk-phase geometry has a unique terahertz spectral fingerprint, and even cases where the packing between two polymorphs is very similar, there is often a dramatic reconfiguration of the terahertz vibrational density of states when transitioning between the two structures.[19] Thus, in order to effectively interpret experimental terahertz spectral data, additional analyses are required.

Over the last decade, methods for assigning and interpreting terahertz spectra have advanced significantly, in line with the growing use of terahertz spectroscopy, providing significant insight into many condensed phase phenomena.[5,20–28] For example, the determination of low-frequency vibrations in organic semiconductors, in tandem with experimental terahertz spectra, has enabled a more thorough understanding of the

This journal is © the Owner Societies 2021

effect of low-frequency vibrations on charge carrier mobilities in these materials.[15,16] However, such insight is entirely dependent upon the correct prediction of both the vibrational frequencies as well as the associated mode-types, which is fundamentally related to the ability of the simulations to reconstruct the potential energy hypersurface to a level of accuracy that enables a proper determination of the weak forces responsible for terahertz dynamics. Over the past two decades there have been a number of advances that have dramatically improved the description of terahertz dynamics,[29] including the determination of IR intensities in periodic simulations,[30] the incorporation of dispersion forces,[31,32] more advanced basis sets,[33,34] force fields,[35] density functionals,[36] and so on. But, by-far the most critical to accurate terahertz analyses has been the development of robust periodic boundary condition simulations.

For the analysis of crystalline solids, periodic boundary conditions have been demonstrated to successfully reproduce terahertz spectra with a high degree of accuracy, as the long-range forces present in the solid are effectively captured by the simulation.[29] However, due to the complexity and (assumed) increased computational cost of periodic boundary condition simulations, gas-phase calculations involving clusters of molecules have been employed in studies describing terahertz vibrations, with varying levels of apparent success.[37–55] It is important to note that, in general, such assessment is based solely on the position of the calculated transitions, with little focus on the actual motions involved or their accuracy. However, there is a lack of comparison in the literature between these methods, and therefore this work aims to assess how gas-phase simulations perform in regard to reproducing not only the experimental terahertz spectra, but also the prediction of the vibrational mode-types. This is of critical importance, as the correct modeling of terahertz spectra implies that the simulation is fully capturing all of the interatomic forces with a high-degree of accuracy. When this criterion is met, experimental terahertz spectra can be used to validate the simulation, enabling access to many related properties that might be difficult to measure experimentally, for example thermodynamic parameters,[28] or interatomic forces.[14] These conditions, especially when coupled with rigorous experimental investigations such as isotopic labeling, temperature-dependent terahertz spectroscopy, and complimentary low-frequency Raman spectroscopy, lead to a powerful methodology for describing dynamic processes with atomic-level precision.

2 Principles and background

2.1 History of terahertz spectroscopy as a tool for the chemical sciences

Terahertz radiation has been used in various capacities for much of the twentieth century, although technological difficulties in its generation and detection made it an elusive laboratory technique. Consequently, the terahertz region of the electromagnetic spectrum was referred to as the "terahertz gap."[56] The terahertz sciences grew out of efforts to measure ultrafast electrical signals, which in turn evolved into the generation and detection of free-space terahertz radiation.[3] While initial pioneering work utilized boutique laser sources and photoconductive antennae,[57] the advent of improved ultrafast lasers led to an increase in research related to terahertz radiation, as the femotosecond optical pulses enabled many lab-based methods to both generate and detect terahertz radiation.[56] Such a discovery lowered the barrier to terahertz experiments, and the general application of terahertz technologies began to flourish.[58]

Expanding upon the initially used photoconductive antennae, new techniques based on non-linear crystals (e.g., ZnTe and GaP), such as optical rectification[59,60] and free-space electro-optic sampling,[61] led to robust tools for performing terahertz experiments in traditional academic laboratories.[62] More recently, advances in terahertz technology have resulted in countless new generation and detection schemes, with some of the more popular methods including improved photoconductive antennae, spanning a number of new materials and shapes,[63] as well as nonlinear crystals, such as 4-dimethylamino-N-methyl-stilbazolium tosylate (DAST),[64] (4-hydroxystyryl)-5,5-(dimethylcyclohex-2-enylidene)malononitrile (OH1),[65] lithium niobate (LiNbO$_3$),[66] and lithium tantalate (LiTaO$_3$),[67] to name a few, as well as air-plasma generation and detection schemes.[68,69] These sources are resulting in terahertz spectrometers that are capable of covering an ultrabroad spectral bandwidth (>3 THz) with higher conversion efficiencies compared to traditional sources. Finally, in recent years quantum cascade lasers (QCLs) have become an area of intense study, with advances enabling high-powered narrowband – and often tunable – terahertz sources.[70]

Early experiments in the terahertz sciences spanned a range of disciplines and applications. Some of the earliest experiments using terahertz radiation involved the study of gas-phase rotational dynamics – effectively an extension of microwave spectroscopy to higher frequencies.[71] For example, an early significant study produced a definitive measurement of the rotational spectrum of water vapor in the range of 0.2–1.45 THz, extending the assignment beyond the bandwidth of typical microwave spectrometers.[72] Other notable achievements in high-resolution rotational spectroscopy using terahertz technology include the measurement of rotational transitions in molecular oxygen isotopologues, and highly-accurate measurements of the rotational transitions of the NH$_2$ anion, critical to the subsequent investigation of interstellar spectroscopic measurements made by the Herschel Space Observatory.[73–75] More recently, terahertz QCLs have been used to perform ultra-high resolution gas-phase spectroscopy, with a reported resolution of <0.5 MHz (5×10^{-7} THz), with some studies even suggesting that QCLs can simultaneously act as both the emitter and receiver module for high-resolution spectroscopy – enabling a compact spectrometer design that is suitable for space-based applications.[76,77]

A second area of terahertz spectroscopy that was quickly recognized leveraged the time-domain nature of most terahertz spectrometers. Because terahertz radiation is generated using ultrafast laser pulses, time-resolved terahertz spectroscopy quickly became a powerful tool for investigating the dynamics

This journal is © the Owner Societies 2021

Phys. Chem. Chem. Phys., 2021, **23**, 20038–20051 | **20039**

of materials; in particular, semiconductors. Terahertz radiation is strongly attenuated by free charge-carriers, and thus optical pump-terahertz probe spectroscopy (OPTPS) became a powerful method for characterizing the charge carrier dynamics of semiconductors with sub-picosecond temporal resolution.[3] Over the years there have been countless insight into carrier dynamics using OPTPS, ranging from the determination of carrier lifetimes – and by-extension, mobilities[78–80] – to the quantification of electron–phonon coupling in perovskite crystals.[81,82] This method has shown growth and utility over the years, with new developments occurring to-date. For example, a recent report highlighted that the charge-carrier dynamics in metal–organic frameworks can be obtained simply by using a powdered sample and a tape cell, making the determination of such data straightforward from a sample-preparation standpoint.[83]

Outside of these two illustrative spectroscopic examples, the terahertz sciences have evolved greatly over the years, yielding a rich and diverse subset of applications, owing to the unique combination of the time-domain nature of terahertz generation, the properties of terahertz waves, and the terahertz response properties of materials. For example, the transparency of many materials to terahertz radiation, coupled with pulsed generation and detection, has provided an opportunity for terahertz pulsed imaging, which has proven to be valuable for the analysis of pharmaceutical coatings,[84,85] security and defense,[86] and the preservation of fragile artwork.[87] Recently, terahertz radiation is also being exploited for its use in telecommunications, as the higher frequencies (compared to current wireless communication standards) result in greatly increased bandwidth and speeds – making terahertz the successor to the 5G standard.[88] But by-far, one of the most widely adopted uses of terahertz radiation is vibrational spectroscopy, and in particular, condensed phase spectroscopy.

2.2 Terahertz vibrational spectroscopy

While terahertz spectroscopy was first applied to gases,[72] by far the most widely adopted application of terahertz spectroscopy is in the condensed phase.[13–15,17,28] In this regard, terahertz vibrational spectroscopy can be thought of as an extension of the more common mid-IR vibrational spectroscopy (*e.g.*, FTIR) to lower frequencies. While far-IR spectroscopy had been performed over the course of the 20th century, the advent of terahertz time-domain spectroscopy (THz-TDS) instruments around the turn of the century reduced the barrier to accessing this region of the electromagnetic spectrum, and its popularity grew accordingly.

All vibrations in molecular systems are governed by the same set of conditions and selection rules, with the frequency of a given vibration dictated by the forces and masses involved in the motion, as shown in the solution of the harmonic oscillator Schrödinger equation,

$$E_v = \hbar\omega\left(\nu + \frac{1}{2}\right) \tag{1}$$

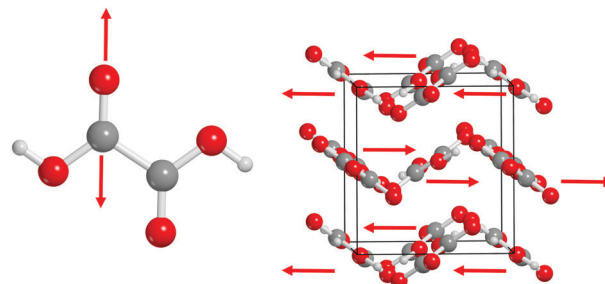$$\omega = \sqrt{\frac{k}{\mu}} \tag{2}$$

Fig. 1 Illustrations of a typical functional group vibration observed in the mid-IR (left) and intermolecular vibration observed in the terahertz region (right), with sample displacements shown with red arrows.

where E_v is the energy of the νth vibrational level, k is the vibrational force constant, and μ is the reduced mass. Thus, while mid-IR techniques probe (relatively strong) interactions, for example covalent bonds, terahertz spectroscopy probes weaker interactions, for example torsional motions of polymer side chains or hindered (rigid-body) translational motions of entire molecules in the condensed phase, as illustrated in Fig. 1.

Unfortunately, while gas- and liquid-phase materials exhibit terahertz vibrational motions, the fact that each individual molecule exists in a different configuration and overall chemical environment leads to a wide-range of terahertz transitions, which often results in a broad absorption feature commonly referred to as the vibrational density of states.[89] While there exists a large body of work in this area, the lack of discrete terahertz absorption features in disordered media limits analyzing atomic-level details from the experimental data without significant efforts.[90] On the other hand, crystalline systems present an ideal medium for performing THz-TDS experiments, as each individual unit cell contains identical molecular conformations and chemical environments, repeated over the entire sample, leading to well-defined vibrational transitions and motions (*i.e.*, phonons) that occur at the same (or nearly the same) frequency for each unit cell.

The dependence of terahertz vibrational transitions on not only the molecular conformation, but also the long-range structure, has made terahertz vibrational spectroscopy an ideal tool for characterizing the dynamics, and by extension, the structures, of crystalline polymorphs.[91] While terahertz spectroscopy is, in itself, not a structural probe; terahertz spectroscopy can be considered a complement to X-ray diffraction. As such, terahertz spectroscopy is an immensely useful tool for the characterization of crystalline materials, rivaling X-ray diffraction in some cases, and surpassing X-ray diffraction in acquisition time.[23,25–27,91]

But while the ability of terahertz vibrational spectroscopy to characterize weak forces and complex dynamics in crystals is one of its most significant assets, it simultaneously leads to its most unfortunate aspects, namely, difficulties in interpreting and assigning the experimental spectra. As mentioned, each individual solid exhibits a unique terahertz spectrum, governed by a complex combination of forces, which ultimately does not

20040 | *Phys. Chem. Chem. Phys.*, 2021, **23**, 20038–20051

This journal is © the Owner Societies 2021

result in any functional/structural-motif-specific vibrations or trends, unlike in the mid-IR. For example, except for the relatively-rare case of isomorphic solids (crystals with a different chemical composition but the same overall structure),[92,93] it is not possible to compare terahertz spectra from two different materials – unlike analyzing spectral peak shifting in the mid-IR – as each solid has a completely unique spectral fingerprint at terahertz frequencies. Therefore, the assignment of terahertz vibrational spectra requires additional analysis, which is most often accomplished through the use of simulation methods.

2.3 Computational assignment of terahertz spectra

Unlike the mid-IR, which have well defined functional-group specific transitions, terahertz vibrations are unique to each individual solid, necessitating computational assignment. Complicating matters further is the nature of terahertz vibrations, which involve long-range weak forces and motions involving large numbers of atoms that are often of mixed mode types. Thus, where mid-IR vibrations are generally governed by the strength of a covalent chemical bond and transition frequencies can be readily predicted based on the identification of the molecule alone, for terahertz analyses, the entire solid (*i.e.*, periodicity) must be considered in order to accurately capture all of the forces that result in the observed vibrational transitions.

Therefore, the assignment of terahertz spectra is, in itself, often more complex than the corresponding experimental measurement. Low-frequency vibrational transitions arise from extremely weak long-range forces (k), in tandem with larger bodies (*i.e.*, entire molecules) constituting the reduced masses (μ) involved in the oscillation (see eqn (1)). Because the mode-types of terahertz vibrations are unique to the studied material and depend on some of the weakest forces in the solid, a highly-robust theoretical method must be used to capture these interactions accurately. Over the years, solid-state density functional theory (DFT), which incorporates periodic boundary conditions, has proven to be an effective methodology, as it fully takes into account the long-range forces found in crystal-line solids.[94] In addition, related methods, such as periodic molecular dynamics simulations, have also been shown to be suitable for the reproduction of experimentally observed terahertz spectra.[95,96]

However, many recent studies have used *ab initio* gas-phase simulations to assign experimental condensed phase terahertz spectra, with varying levels of apparent success.[37–55,97–99] While the errors of these isolated-cluster calculations have been discussed by Tomerini and Day,[100] a number of studies using exactly these methods have been published since then. It is important to note that in almost all of these cases the discussed 'agreement' with experiment is largely based upon the position of calculated vibrational transitions, with little focus placed upon the accuracy of the predicted mode-types – critical for gaining deeper insight into the way terahertz motions influence bulk material properties, for example. While to many in the community it is patently obvious that single-molecule or cluster models are inadequate tools for the simulation of crystalline terahertz spectra, there continues to be a large number of

publications produced each year that use these exact methods, with no reasonable justification.[52,53,97,99,101–109] Clearly, there is a salient discontinuity in the understanding of the assignment of crystalline terahertz spectra with DFT, which could be attributed to the distinct absence of a systemic study detailing the discrepancies of gas-phase simulations and the experimental crystalline terahertz spectra they seek to assign. Therefore, this work aims to assess how gas-phase simulations reproduce terahertz spectra, as well as predict the corresponding vibrational mode-types.

3 Results and discussion

3.1 Overview

Due to the sensitivity of terahertz spectra to weak, long-range, non-covalent forces, a series of materials exhibiting a variety of these intermolecular forces were chosen. The vibrational spectra of these crystals were then calculated using fully-periodic DFT simulations using the Crystal17 software package,[110] as well as with gas-phase DFT simulations on clusters of various sizes using Gaussian09.[111]

The experimental and solid-state DFT-predicted terahertz spectra of the materials chosen for this study are shown in Fig. 2. Specifically, oxalic acid – one of the simplest organic solids – was chosen based on its prevalent hydrogen bonding and relatively small size. Its dihydrate was also chosen to explore how the inclusion of co-crystallized water molecules influences the simulation of the spectra, particularly in the gas-phase clusters. Finally, two polymorphs of lactose were selected, as they represent common standards for terahertz spectroscopy[112] and exhibit a range of interactions, including significant London dispersion forces and the presence of flexible torsional angles.

Solid-state simulations often employ experimental crystal structures as input geometries, which are then optimized prior to the calculation of the vibrational dynamics.[29] This represents a rather straightforward methodology, as it leaves no room for user input, assuming a well-behaved material with an accurate experimental crystal structure. On the other hand, the gas-phase cluster simulations require a choice by the user, who must decide on the cluster size, configuration, number of molecules, and so on.

This choice, however, presents a rather significant philosophical question. For a molecular crystal defined by an infinite repetition of a group of atoms (or molecules) across space, what one single portion of the system, in its isolation, best represents the delicate interplay of weak intermolecular forces that drive terahertz vibrations? While it may seem intuitive to derive this portion from an experimental crystal structure, the posited question persists, what section of the crystal structure is a sufficient representation? If a molecule is simply translated or rotated in the unit cell, is its inclusion necessary? Is there an intermolecular distance that demands the inclusion or exclusion of a section of the crystal? Is even a single unit cell sufficient? Along with a surplus of other considerations, all of these inquiries are immensely difficult to

This journal is © the Owner Societies 2021

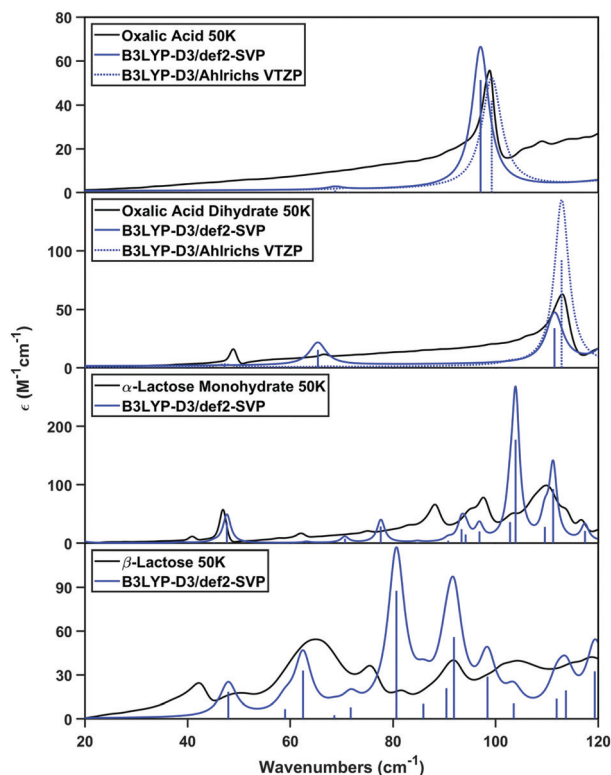*Phys. Chem. Chem. Phys.*, 2021, **23**, 20038–20051 | **20041**

Fig. 2 Cryogenic experimentally observed terahertz spectra (black) and theoretical spectra predicted with the B3LYP-D3/def2-SVP method (blue) for anhydrous oxalic acid, oxalic acid dihydrate, α-lactose monohydrate, and β-lactose. The frequencies of the theoretically produced spectra using the def2-SVP basis set have been scaled by a factor of 0.9, while the spectra predicted using Ahlrichs VTZP basis set has been scaled by 0.94 for oxalic acid dihydrate, while the theoretical anhydrous oxalic acid spectrum is unscaled.

answer without a rigorous theoretical investigation, which will almost certainly differ for any given individual crystalline system. While it may be the case that a general convergence of vibrational transition frequencies and mode-types produced by a variety of models can offer enough insight to assign an experimental crystalline terahertz spectrum, to the best of our knowledge, there has been no such examination.

Thus, in order to explore the aforementioned questions, as well as plainly demonstrate both how any construction of these clusters is an insufficient representation of a periodic system, as well as the immense sensitivity of terahertz spectra to any changes introduced by the selected model, gas-phase simulations were performed using geometries directly extracted from experimental crystal structures, as well as clusters generated in differing manners, for example single-layered sheets, multi-layered stacks, and in the case of oxalic acid dihydrate, subtle changes to only the initial water molecule configuration while keeping the organic portion fixed. Though it is likely impossible for non-crystalline cluster geometries to reproduce experimental spectra, these clusters serve to demonstrate the sensitivity of low-frequency vibrations to initial geometries.

In order to effectively compare the periodic and gas-phase results, the exact same theoretical parameters were used for all

simulations. Specifically, the B3LYP density functional,[113] along with the D3 dispersion correction,[114,115] was used with the def2-SVP basis set.[116] While the overall agreement with the experimental terahertz spectra and the periodic simulations is good after global scaling of the theoretical spectra for all systems, it is possible to improve the accuracy of the vibrational simulations by using a larger triple-zeta basis set (Ahlrich's VTZP[117]), as shown for oxalic acid and its dihydrate in Fig. 2. The larger basis set results in a better agreement with the experiment without requiring scaling, however it is important to note that the improvement is largely due to the better overall description of the intermolecular forces, as evidenced by the errors in the calculated unit cell parameters for the two methods, with the double-zeta basis set producing larger errors ($\sim$2.3%) compared to the triple-zeta basis set ($\sim$0.79%), which is what necessitates a larger scale factor for the smaller basis set, as discussed in previous work.[94] Because the goal of this work is to compare theoretical methods, and because the smaller basis set only results in a larger overall global shifting of the spectra, coupled with the drastically increased computational cost of the triple-zeta basis set, the def2-SVP basis set was utilized throughout this study. To compare the theoretical spectra, the predicted IR-active vibrational transition frequencies and associated intensities were fit with Lorentzian functions with fixed FWHM values of 2.2 cm^{-1}, unless stated otherwise.

3.2 Predicting accurate mode-types in anhydrous oxalic acid

The ability of simulations to capture the weak and long-range forces found in simple crystalline solids is critical to the success of the method, and the subsequent interpretation of the experimental results. Thus, anhydrous oxalic acid, one of the simplest hydrogen-bonded organic solids, was selected as the first system for study. Anhydrous oxalic acid crystallizes in the orthorhombic *Pbca* space group, with 4 molecules in the unit cell, and lattice parameters of a = 6.49 Å, b = 6.06 Å, c = 7.80 Å, and $\alpha = \beta = \gamma = 90°$, derived from single crystal X-ray experiments conducted at 130 K.[118] The crystalline structure was initially optimized with the fully periodic Crystal17 DFT software package using the def2-SVP/B3LYP-D3 method,[113–116,119,120] which resulted in an average error of the unit cell parameters of 2.30%, compared to reported single crystal X-ray diffraction data.[118]

The results of the fully periodic vibrational simulation are shown in Fig. 3A. The simulation predicts 9 IR-active modes below 250 cm^{-1}, and only two between 0–150 cm^{-1}, occurring at 76.44 and 107.85 cm^{-1}. These two modes correspond to antisymmetric unidirectional molecular translations of adjacent planes along the *c*-axis, and small translations along the *a*-axis with torsional motions between the carboxyl groups (Fig. 4A and B), respectively, which is in agreement with the previous assignment of King and Korter.[121]

To first assess the ability of gas-phase simulations to accurately predict both vibrational transition frequencies and mode-types, a single molecule of oxalic acid underwent geometric optimization and frequency analysis with Gaussian09[111] using the same computational parameters as the periodic boundary condition calculations, producing the spectrum
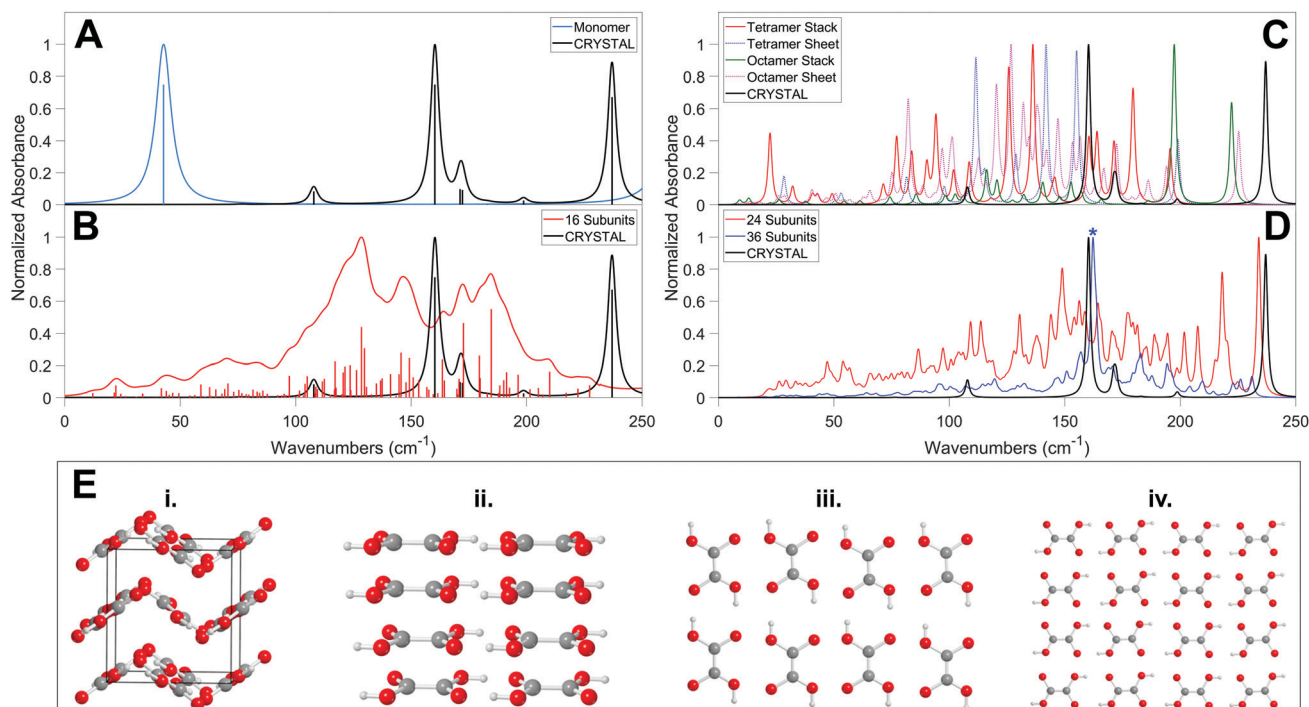
Fig. 3   Predicted anhydrous oxalic acid low-frequency spectra. (A) Gas-phase monomer (blue) and solid-state (black) theoretical spectra. (B) Theoretical spectra generated from gas-phase 16-subunit cluster (red) and solid-state (black). (C) Sheet and stack cluster constructions of tetramer and octamer clusters, with a narrowed FWHM (1 cm^{-1}) for clarity. (D) Theoretical spectra of higher ordered clusters derived from experimental X-ray measurements, with a narrowed FWHM (1 cm^{-1}) for clarity. (E) Structures of oxalic acid crystalline unit cell (i), octamer stacked cluster (ii), octamer sheet cluster (iii), and 16-subunit sheet cluster (iv).

shown in Fig. 3A. This simulation yields a single IR active mode in the low-frequency region at 42.83 cm^{-1}, and ultimately fails to reproduce the experimental spectrum. Furthermore, the primary motion associated with this mode involves

intramolecular torsional motion between the carboxyl groups (Fig. 4B). A similar motion is observed in the mode produced by the periodic simulation at 107.85 cm^{-1} (+60.29% deviation), which is blue-shifted, compared to the gas-phase simulation,
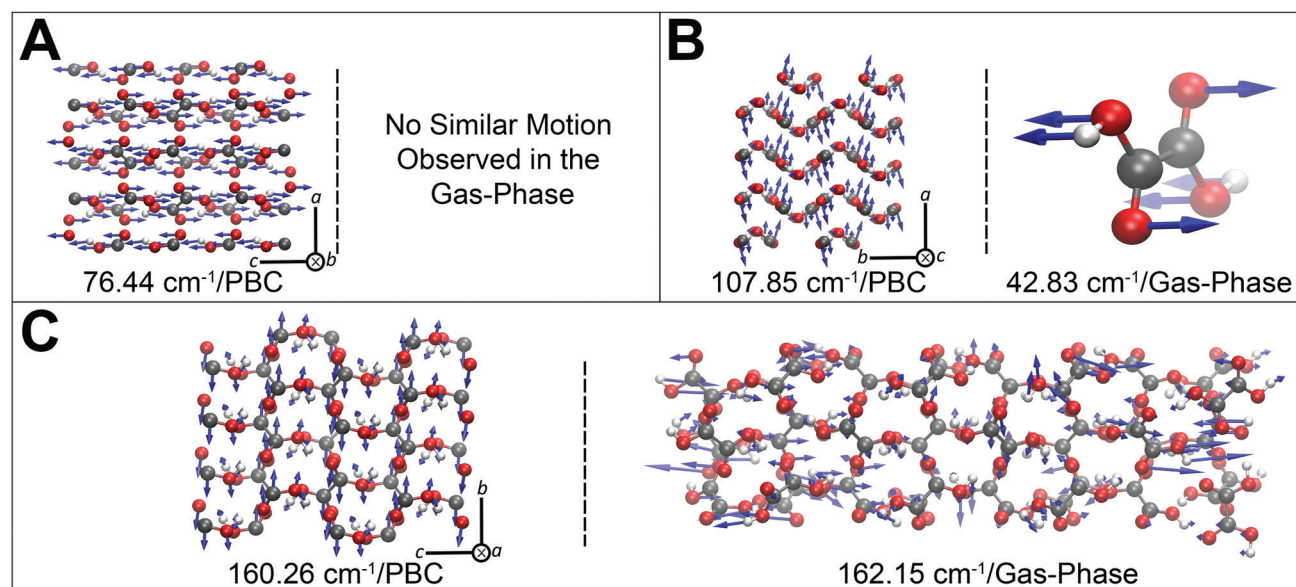

Fig. 4   Predicted motions of low-frequency vibrations of anhydrous oxalic acid, with atomic displacements visualized with blue arrows. (A) Motions of 76.44 cm^{-1} vibrational mode predicted from periodic DFT. (B) Motions of 107.85 cm^{-1} and 42.83 cm^{-1} vibrational modes predicted from periodic and gas-phase DFT, respectively. (C) Motions of 160.26 cm^{-1} and 162.15 cm^{-1} vibrational modes predicted from periodic and gas-phase DFT, respectively.

due to the incorporation of intermolecular forces in the periodic simulation.

However, it is important to note that the lack of intermolecular forces results in two differing, yet related, consequences. Firstly, the calculated motion demonstrates no intermolecular character (*i.e.*, translation of adjacent molecules), which is present in the mode at 107.85 cm^{-1} predicted by the periodic simulation. While the two mode-types exhibit similarities in the intramolecular dynamics, the overall motion of the modes contrast. Secondly, the lack of intermolecular forces significantly softens this mode, leading to the large deviation in the calculated transition frequency between the two methods. It becomes clear that an isolated molecule fails to describe the experimental terahertz spectrum, as well as the encompassing depiction of the associated motions.

While it is obvious that the introduction of more molecules to the simulation is necessary, the aforementioned thought experiment must be revisited. Which gas-phase model ought to be chosen? This selection should stem from an understanding of how cluster size and orientation affects the prediction of low-frequency vibrations, which again, is largely unknown. Therefore, to incorporate the weak intermolecular forces and allow for intermolecular motions in the gas-phase simulations, clusters of increasing size and configurations were prepared. In doing so, the effects of the size of the simulation, as well as the selected input geometry, can effectively be assessed.

Clusters were constructed in three manners: direct extraction from the reported single crystal X-ray structure (Fig. 3E(i)), hydrogen-bonded dimers forming stacks (Fig. 3E(ii)), and planar sheets (Fig. 3E(iii and iv)). Each model underwent geometric optimization with no constraints followed by vibrational simulations, with a sample of the spectra presented in Fig. 3B–D. Predicted spectra and utilized cluster geometries are provided in the ESI.†

Across the differing constructions of the clusters, it generally the case that as the number of molecules in the gas-phase simulation increases, more low-frequency vibrations are predicted – an unsurprising result given the direct relationship between the number of atoms and vibrational degrees of freedom. However, the calculation of more low-frequency normal modes does not inherently imply better agreement with the periodic simulation, or experimental data. In fact, the opposite effect is plainly visualized in Fig. 3B–D, with the spectra predicted by these clusters exhibiting features that are entirely absent in the results of periodic simulation. For emphasis of this effect, in contrast to the 9 modes predicted in the range of 0–250 cm^{-1} from the periodic calculation, a total of 106, 162, and 246 vibrational modes are predicted from the clusters containing 16, 24, and 36 molecules, respectively. As evidenced by these simulations, gas-phase simulations can predict an abundance of low-frequency vibrations, which will almost certainly offer some overlap with the experimental spectrum, based solely upon the position of transition frequency energies and intensity values. However, assignment by this criteria alone is highly problematic, especially when there exist just as many (if not more) predicted modes in

prominent disagreement with the experimental data, and can quickly lead to inaccurate and physically meaningless results.

It is reasonable to assume that as gas-phase simulations more closely resemble the crystalline environment, the resultant predictions of terahertz dynamics become more accurate, which can be validated with the experimental spectrum. Accordingly, clusters derived directly from a supercell of the oxalic acid crystal structure were designed to assess this presumption. Moreover, it would be expected that clusters including more molecules (*i.e.*, the 36-subunit cluster) would offer the strongest agreement, as the larger cluster size would offer more character of the weak forces that give rise to terahertz vibrations. The results of this simulation is visualized in Fig. 3D.

It can be clearly observed that the 36-subunit cluster is unable to fully reproduce the accuracy demonstrated by periodic simulation, which is also observed in the smaller 24-subunit clusters generated in the same manner. Instead, only apparent agreement with individual features of spectrum predicted by the solid-state calculation is observed. Specifically, the 36-subunit cluster predicts an intense transition occurring at 162.15 cm^{-1}, seemingly reproducing the absorption feature at 160.27 cm^{-1} predicted by the periodic simulation (Fig. 3D). For these modes specifically, the periodic simulation exhibits a concerted motion, composed of antisymmetric molecular translations primarily along the *b*-axis with a small contribution of translation along the *a*-axis, while the cluster offers no such concerted motion, with atomic motions differing in magnitude and direction across each molecule in the cluster (Fig. 4C). Upon close inspection, there does seem to be a degree of similarity between the two mode-types, where the most surrounded atoms in the cluster begin to depict the correct direction of atomic displacement. However, without the guide of the periodic calculation, it would be entirely impossible to validate this seemingly-accurate motion in only a portion of the simulated molecules, only further complicating the task of assigning experimental spectra with cluster simulations. Similar effects are observed in the 24-subunit cluster simulations, where one calculation predicts an intense transition occurring at 230.98 cm^{-1}, closely resembling the feature predicted by the periodic simulation at 236.93 cm^{-1} (Fig. 3D). However, the motions of these vibrations offer no similarity, as visualized in the ESI.† Moreover, the 24-subunit clusters differing only in spatial sampling of the crystalline supercell each produce a unique terahertz spectrum, provided in the ESI,† which fail to converge to similar values. Finally, it is important to note that it is certainly possible that given a large enough cluster, it might be possible to reach agreement with the periodic simulations. However, a model such as this would certainly exceed the limits of modern computational chemistry, and the use of periodic simulations is a much more straightforward method to obtain accurate results.

In a general case for these clusters, the predicted vibrational modes depict more intermolecular character as the size of the cluster increases, but fail to replicate the characteristic lattice vibrations predicted from the periodic simulation, with atomic motions differing between each individual molecule in the cluster. In addition to providing inadequate representations

20044 | *Phys. Chem. Chem. Phys.*, 2021, **23**, 20038–20051

This journal is © the Owner Societies 2021

of terahertz vibrations, the 36-subunit cluster was significantly more computationally costly, wherein $3N$ displacements are required to generate the Hessian matrix from which normal modes are calculated following diagonalization, where N is the total number of atoms included in the simulation. Solid-state DFT exploits the symmetry of the crystalline system, wherein $3N$ displacements are required for the same process, but N is the number of atoms included only in the symmetry-independent unit of the primitive cell.

Additionally, it is clear that the gas-phase calculations produce optimized geometries that deviate from the crystalline equilibrium positions, even when experimental coordinates are used as input geometries (Fig. 4C), which inherently alters the desired long-range structure. However, the intermolecular distances determined by hydrogen-bonding are similar in the cases of the 36-subunit cluster and periodic calculations, producing average hydrogen-bond distances of 1.71 Å and 1.63 Å, respectively. Such a result could be mistaken as an accurate capture of inter-molecular forces, but this is simply a demonstration of the ability of DFT to accurately capture the electrostatic forces governing hydrogen-bonding. Crystalline anhydrous oxalic acid exhibits a specific direction of hydrogen-bonding, namely in the b–c-plane of the unit cell in a chevron pattern, constituting layers of molecules stacked along the a-unit cell axis (Fig. 4B). However, the lack of boundary conditions in the cluster simulations create artificial hydrogen-bonding contacts at the cluster boundaries, leading to large deviations from the crystalline geometry, which sequentially predicts inaccurate terahertz vibrations. This is quantitatively demonstrated in the torsional angle between carbonyl groups of the oxalic acid molecule, which the periodic calculation accurately reproduces (180°), but varies for each molecule in the 36-subunit cluster, with an RMSD value of 43.86°.

It is possible that if stricter constraints are placed upon the geometries of these clusters, these simulations could more closely resemble the crystalline environment, and by extension, produce more accurate mode-types. To assess this effect, an expanded unit cell containing 13 molecules of anhydrous oxalic acid was extracted and symmetry imposed, with the symmetry maintained throughout the optimization. This simulation ultimately resulted in both a spectrum in disagreement with the periodic calculation, with inaccurate mode-types of vibrational modes, as well as a cluster geometry that deviates significantly from the experimentally derived crystal structure, as shown in the ESI.† These errors arise from the simple fact that it is not possible to maintain crystalline symmetry in a gas-phase simulation. While one might be tempted to perform a frequency analysis without performing an optimization, this is bad practice, as it results in the generation of a large number of imaginary modes – in this case, 62 negative frequency modes out of a total of 306 vibrations, invalidating the results of this calculation entirely.

The results of these cluster simulations offer two primary findings. Firstly, the only degree of accuracy in both vibrational transition frequency and mode-type simultaneously was observed in the 36-subunit cluster. Even then, this was only apparent for one portion of the cluster, for a single low-frequency normal mode. From this, one could come to the conclusion that in the case of an even larger (and by consequence, considerably more computationally costly) cluster, it is possible that more atoms would depict the correct mode-type. However, it would still be the case that molecules less surrounded in the cluster, especially at the cluster boundary, would fail to depict the correct mode-type, and there would be no meaningful manner in which to separate accurate and inaccurate atomic motions without a periodic simulation. Solid-state calculations address this directly, as the system is modeled over infinite space, with significantly less cost than the performed cluster calculations. Secondly, there is a distinct lack of convergence of the predicted terahertz spectra, seen in both the results of the 24-and 36-subunit clusters, as well as the differing orientations of the 24-subunit clusters. This suggests that not only is the produced terahertz spectrum sensitive to the number of molecules included in the simulation, but also their respective orientation, even when extracted from crystalline equilibrium positions.

Addressing the latter, it is crucial to illustrate exactly how sensitive the predicted terahertz spectra are to the initial user selected geometry. The stack-and sheet-based clusters of oxalic acid (Fig. 3(ii–iv)) swiftly provide this demonstration, with these simulations producing a wide variety of low-frequency modes, with large differences in transition frequency, intensity, and mode-type (Fig. 3B and C). Though these spectra are highly variable, even these clusters, with virtually no resemblance to the experimental crystal structure, result in low-frequency vibrations that fall within close ranges of modes predicted by the periodic simulation, which cannot and should not be mis-taken as apparent agreement. Further, it could be rationalized that each class of these clusters should converge to similar groupings of low-frequency vibrations based upon a common orientation, no such phenomenon is observed, emphasizing the responsiveness of the theoretical result to initial geometry. The results of these simulations, in tandem with clusters derived directly from crystalline geometries indicate that while a gas-phase cluster simulation may produce vibrational frequencies falling within a close range of modes predicted from periodic simulations or experimental spectra, this does not mean the simulation is physically meaningful, and any apparent agreement exists only coincidentally. However, at higher frequencies (namely the mid-IR region), the results of the gas-phase and periodic simulations converge to similar vibrational transition frequencies and mode-types, as shown in the ESI.† Such agreement stems from the corresponding functional group specific vibrations, which are significantly less reliant upon long range structure.

3.3 The role of subtle interactions on terahertz spectra

The study of anhydrous oxalic acid demonstrates the sensitivity of low-frequency vibrational frequencies and mode-types to both the correct representation of the forces, as well as the initial three-dimensional structure. However, without question, the structures investigated above are significantly different, and it might seem obvious that they would ultimately produce

This journal is © the Owner Societies 2021

Phys. Chem. Chem. Phys., 2021, **23**, 20038–20051 | **20045**

different terahertz spectra. In order to further study the sensitivity of low-frequency spectra to more-subtle structural differences, oxalic acid dihydrate was investigated. Here, instead of generating different bulk arrangements of the oxalic acid molecules, we have chosen to take a dimeric-pair and fix its geometry. Subsequently, we have purposefully generated structures with only the positions of four water molecules varied, as this is how one might proceed when attempting to simulate the terahertz spectrum of a co-crystal (or hydrate) with cluster models. We emphasize that our goal here is not to identify a 'correct' structure, but rather to highlight how sensitive the resulting spectra are to the initial geometric model. The structures chosen are shown in Fig. 5A(i–iii), and even with only subtle changes in the starting positions of water molecules, the predicted theoretical terahertz spectra vary significantly, with each dimer cluster producing a unique spectrum (Fig. 5B). Such a result indicates that even slight changes in the geometry, which may not be immediately identifiable, are able to directly and strongly influence low-frequency spectral predictions. This finding is of practical importance, as clearly the initial user-generated geometry significantly influences the final simulated low-frequency spectra.
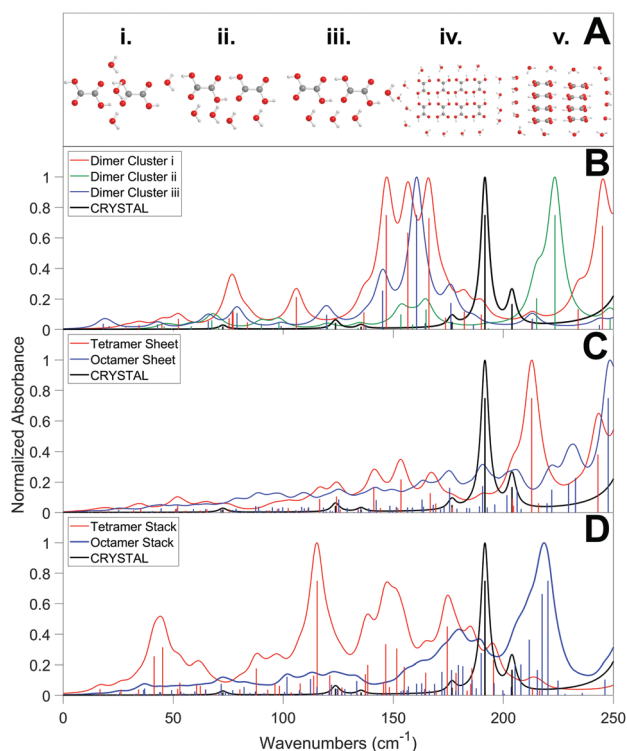

Fig. 5 Predicted oxalic acid dyhydrate low-frequency spectra. (A) Initial gas-phase geometries of oxalic acid dihydrate. (i–iii) Representative oxalic acid dihydrate dimer clusters with varied water starting geometries. (B) Low-frequency spectra generated from oxalic acid dihydrate dimers with varied water starting geometries. (C) Low-frequency spectra generated from tetramer and octamer sheet clusters of oxalic acid dihydrate. (D) Low-frequency spectra generated from tetramer and octamer stacked clusters of oxalic acid dihydrate.

As was the case of the anhydrate, larger clusters of oxalic acid dihydrate constructed with differing positions of the oxalic acid molecules (Fig. 5A(iv and v)) produce highly varied low-frequency spectra, which fail to converge to similar values, as visualized in Fig. 5C and D. Again, predicted from clusters with clear deviations from the experimental crystal structure, there exist some spectral features that seem to resemble those of the periodic simulation, but the corresponding mode-types fail to depict the concerted motion of molecules expected of phonons, which are captured in the mode-types of the solid-state simulations, and fall close to experimental frequencies only coincidentally. Even in the case of clusters constructed directly from crystalline geometries, ranging from a single unit cell to extended supercells, the resultant theoretical spectra fail to reach agreement with the results of the periodic simulation and experimental data, as well as predicting vibrational modes that significantly vary from each individual cluster, as visualized in the ESI.†

3.4 Large flexible molecules and polymorphism

Oxalic acid in both its anhydrous and dihydrated forms are small molecules, and the observed intramolecular contributions to low-frequency vibrations primarily exist as torsions and rotations at higher vibrational frequencies (>100 cm^{-1}). In larger molecules, such intramolecular character is significantly less hindered as conformational changes are more easily accessed, and associated motions occur at lower frequencies.[122] Such a consideration is exemplified in molecules able to adopt multiple molecular conformations, such as α-lactose monohydrate and anhydrous β-lactose (Fig. 6A). It is possible that gas-phase simulations are able to more accurately predict low-frequency vibrational frequencies and motions composed of more intramolecular character, and thus the evaluation of gas-phase models was extended to both of these solids.

The periodic simulations for both α-lactose monohydrate and β-lactose are in good agreement with reported terahertz spectra.[123,124] To retain the anomeric differences and consequent long-range forces of the two solids in the gas-phase simulations, clusters of lactose in both forms were constructed from a supercell derived from single crystal X-ray experiments (Fig. 6A), from a single subunit to an octamer.[125,126] Following the trend of oxalic acid, the spectra produced from the gas-phase simulations of both lactose solids (Fig. 6B and C) offer little agreement to the experimental spectra, with an excess of vibrational frequencies compared to the experimental spectrum. Specifically, 37 vibrational modes are predicted in the range of 0–250 cm^{-1} from the periodic calculation of α-lactose monohydrate. The cluster simulation with the most intermolecular character (the octamer cluster) predicts a total of 173 vibrational modes, drastically deviating from the results of the periodic simulation. A similar result is also observed in the β-lactose polymorph, with 32 vibrational modes predicted in the terahertz region, while the largest cluster calculation predicts an excess of 159 vibrational modes. Additionally, the mode types present non-uniform motions throughout the cluster, differing in both magnitude and direction (see ESI†),
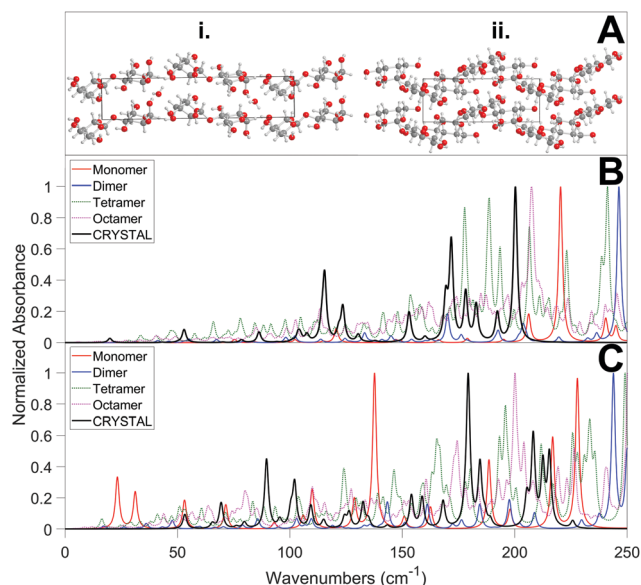
20046 | *Phys. Chem. Chem. Phys.*, 2021, **23**, 20038–20051

This journal is © the Owner Societies 2021

Fig. 6 Predicted α-lactose monohydrate and β-lactose low-frequency spectra. (A) Crystalline unit cell of α-lactose monohydrate (i) and β-lactose (ii). (B) Low-frequency spectra generated from α-lactose monohydrate clusters of size 1–8 subunits with narrowed FWHM values (1 cm^{-1}) for clarity. (C) Low-frequency spectra generated from β-lactose clusters of size 1–8 subunits with narrowed FWHM values (1 cm^{-1}) for clarity.

mimicking the shortcomings observed in the gas-phase simulations of oxalic acid and its dihydrate.

3.5 Misleading physical interpretation with gas-phase simulations

The proper assignment of terahertz spectra can have practical importance, and can strongly influence the interpretation of experimental results. A recent example highlights how improper analysis using gas-phase simulations can lead to incorrect conclusions. In a study by Ajito *et al.*, the freeze-drying dynamics of aqueous NaCl solutions were investigated using THz-TDS, and over the course of the experiment the appearance, and subsequent disappearance, of two spectral features were observed.[39] The authors proposed a mechanism involving the formation of not only sodium chloride dihydrate (NaCl·2H$_2$O) – an established reaction pathway – but also the formation of intermediate NaCl nanoparticles. The authors utilized gas-phase cluster simulations based on molecular dynamics, and subsequently identified two structures that yield spectral features that are in some agreement with the experimental data. The conclusion of the observed NaCl nano-particles was drawn primarily from these simulations. However, as discussed in this Perspective, it is trivial to obtain a spectrum that 'agrees' with an experimental result, by simply varying cluster geometries arbitrarily, and thus this is clearly not an appropriate methodology. In the case of this work, a fully periodic simulation of NaCl·2H$_2$O results in a predicted spectrum that is in excellent agreement with the reported experimental spectrum (Fig. 7), implying that authors instead observed the formation, and sequential dehydration, of bulk
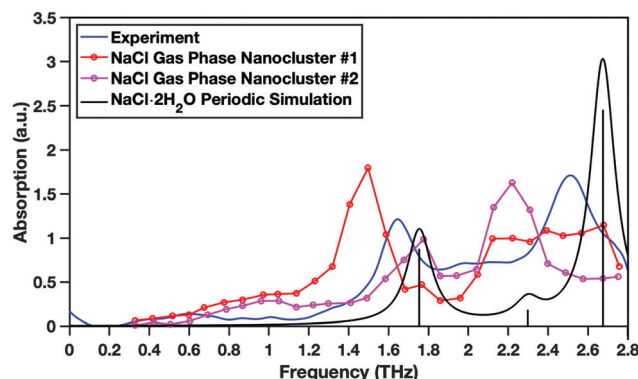

Fig. 7 Reported experimental (blue) terahertz spectrum of aqueous NaCl upon freezing (77 K), and the corresponding reported assignment of the spectrum to two different NaCl nanoclusters simulated using gas phase simulations (red and magenta).[39] The black curve is a periodic simulation of NaCl·2H$_2$O, which is in excellent agreement with the experimental spectrum, representing a much more plausible assignment.

NaCl·2H$_2$O crystals; a much more plausible, and fact-based conclusion than what is described in that work.

4 Conclusions and outlook

Across the solids surveyed in this study, the terahertz spectra generated from gas-phase clusters fail to replicate the simulations performed with periodic boundary conditions, which are in agreement with reported experimental terahertz spectra. Cluster-based simulations especially deviate from experimental spectra in the number of modes predicted in the terahertz region (0–250 cm^{-1}), in which differing motions are localized to specific molecules, rather than the concerted character detailed by vibrations occurring in the terahertz region. Such behavior can be generalized to all vibrations in this region, regardless of spectroscopic selection rules (*i.e.*, both infrared and Raman-active vibrational modes). These discrepancies can be attributed to the lack of incorporation of long-range structures and inter-actions, which are responsible for dictating the terahertz spectra of solids. Thus, while gas-phase cluster simulations that seem to accurately capture the terahertz dynamics of solids can be obtained, they are not physically meaningful, as even subtle changes in the cluster configuration can drastically alter the predicted spectra.

Over the last decade computational advances are enabling highly-accurate atomistic simulations of complex condensed phase materials to be performed. It is a great achievement that there exist robust tools, incorporating periodic boundary conditions, that can accurately reproduce the weak forces responsible for terahertz dynamics. While historically gas phase cluster simulations might have been the only reasonable option for simulating vibrational dynamics, this is no longer the case, and the community should strive to only recognize simulations that are of sufficient quality and rooted in physical phenomena for interpreting low-frequency vibrational spectro-scopic data. Overall, the field of terahertz vibrational spectro-scopy is more accessible than ever, and this understanding

This journal is © the Owner Societies 2021

Phys. Chem. Chem. Phys., 2021, **23**, 20038–20051 | **20047**

should become second-nature as this exciting field grows and matures.

5 Methods

5.1 Experimental

5.1.1 Sample preparation. Anhydrous oxalic acid, α-lactose monohydrate, β-lactose, were purchased and used as received. Oxalic acid dihydrate was obtained by recrystallization from an aqueous solution of oxalic acid, yielding large colorless needlelike crystals.

5.1.2 Terahertz time-domain spectroscopy. Samples for THz-TDS measurements were prepared by mixing with PTFE to a 10% w/w concentration, followed by homogenization *via* pestle and mortar. The powdered mixture was then pressed under 2 tons of pressure in a 13 mm diameter die, furnishing 3 mm thick freestanding pellets. All THz-TDS spectra were acquired using a commercial Teraflash spectrometer (Toptica Photonics AG). Cryogenic (20 K) spectra were collected using a closed-cycle liquid helium cryostat (Cryocool Industries). For each sample, 30 000 time-domain waveforms were collected and averaged, and the resultant waveform underwent Fourier transform to yield a terahertz power spectrum with a spectral resolution of <0.1 cm^{-1}. The reported spectra represent the division of the sample power spectra by the PTFE blank spectra.

5.2 Theoretical

5.2.1 Periodic simulations. Solid-state density functional theory simulations, incorporating periodic boundary conditions, were performed using the Crystal17 DFT software package.[110] The crystalline solids were modeled using the hybrid Becke[119] three-parameter, Lee–Yang–Parr[120] (B3LYP)[113] density functional, coupled with Grimme's DFT-D3 dispersion corrections,[114] including the Becke–Johnson damping function.[115] The atomic orbitals were represented using the split-valence double-ζ def2-SVP basis set.[116] All structures were initially fully optimized (lattice parameters and atomic positions) with no constraints other than the space-group symmetry of the individual solids. In the case of anhydrous oxalic acid, geometry optimizations were also performed with Ahlrich's triple-ζ basis set (VTZP),[117] with three body dispersion contributions. This optimization offered little improvement over the def2-SVP basis set while significantly increasing computational cost, and thus def2-SVP/B3LYP-D3 method was employed in all simulations. Upon complete optimization, vibrational analyses were performed, and infrared intensities were calculated using the Berry-phase method. Energy convergence criteria were set to $\Delta E \leq 10^{-8}$ and 10^{-11} Hartree for the optimization and vibrational calculations, respectively.

5.2.2 Gas phase simulations. Gas phase calculations were performed using the Gaussian09 DFT package[111] employing tight convergence criteria, enforcing an energy criterion of $\Delta E \leq 10^{-13}$ Hartree as well as an ultrafine integration grid. In order to most closely compare the gas phase and periodic simulations, all simulations performed in this manner employed the def2-SVP basis set, and the B3LYP density functional, with Grimme-D3 dispersion corrections.

Conflicts of interest

There are no conflicts to declare.

Acknowledgements

Notes and references

1 H. Sirringhaus, *Adv. Mater.*, 2014, **26**, 1319–1335.
2 K. Ohta, S. Tokonami, K. Takahashi, Y. Tamura, H. Yamada and K. Tominaga, *J. Phys. Chem. B*, 2017, **121**, 10157–10165.
3 C. A. Schmuttenmaer, *Chem. Rev.*, 2004, **104**, 1759–1779.
4 D. Markl, P. Wang, C. Ridgway, A.-P. Karttunen, M. Chakraborty, P. Bawuah, P. Pääkkönen, P. Gane, J. Ketolainen, K.-E. Peiponen and J. A. Zeitler, *J. Pharm. Sci.*, 2017, **106**, 1586–1595.
5 W. Zhang, J. Maul, D. Vulpe, P. Z. Moghadam, D. Fairen-Jimenez, D. M. Mittleman, J. Axel Zeitler, A. Erba and M. T. Ruggiero, *J. Phys. Chem. C*, 2018, **122**, 27442–27450.
6 L. Yu, L. Hao, T. Meiqiong, H. Jiaoqi, L. Wei, D. Jinying, C. Xueping, F. Weiling and Z. Yang, *RSC Adv.*, 2019, **9**, 9354–9363.
7 J. A. Zeitler, D. A. Newnham, P. F. Taday, T. L. Threlfall, R. W. Lancaster, R. W. Berg, C. J. Strachan, M. Pepper, K. C. Gordon and T. Rades, *J. Pharm. Sci.*, 2006, **95**, 2486–2498.
8 N. Y. Tan and J. A. Zeitler, *Mol. Pharmaceutics*, 2015, **12**, 810–815.
9 K. Drużbicki, E. Mikuli, N. Pałka, S. Zalewski and M. D. Ossowska-Chróściel, *J. Phys. Chem. B*, 2015, **119**, 1681–1695.
10 M. T. Ruggiero, J. A. Zeitler and T. M. Korter, *Phys. Chem. Chem. Phys.*, 2017, **19**, 28502–28506.
11 H. Hoshina, H. Suzuki, C. Otani, M. Nagai, K. Kawase, A. Irizawa and G. Isoyama, *Sci. Rep.*, 2016, **6**, 1–6.
12 M. T. Ruggiero, W. Zhang, A. D. Bond, D. M. Mittleman and J. A. Zeitler, *Phys. Rev. Lett.*, 2018, **120**, 196002.
13 M. T. Ruggiero, J. Sibik, R. Orlando, J. A. Zeitler and T. M. Korter, *Angew. Chem., Int. Ed.*, 2016, **55**, 6877–6881.
14 P. A. Banks, J. Maul, M. T. Mancini, A. C. Whalley, A. Erba and M. T. Ruggiero, *J. Mater. Chem. C*, 2020, **8**, 10917–10925.
15 G. Schweicher, G. D'Avino, M. T. Ruggiero, D. J. Harkin, K. Broch, D. Venkateshvaran, G. Liu, A. Richard, C. Ruzie, J. Armstrong, A. R. Kennedy, K. Shankland, K. Takimiya, Y. H. Geerts, J. A. Zeitler, S. Fratini and H. Sirringhaus, *Adv. Mater.*, 2019, **31**, 1902407.
16 T. Otaki, T. Terashige, J. Tsurumi, T. Miyamoto, N. Kida, S. Watanabe, T. Okamoto, J. Takeya and H. Okamoto, *Phys. Rev. B*, 2020, **102**, 245201.

17 T. Tanno, Y. Watanabe, K. Umeno, A. Matsuoka, H. Matsumura, M. Odaka and N. Ogawa, *J. Phys. Chem. C*, 2017, **121**, 17921–17924.

18 W. Zhang, Z. Song, M. T. Ruggiero and D. M. Mittleman, *Cryst. Growth Des.*, 2020, **20**, 5638–5643.

19 A. J. Zaczek and T. M. Korter, *Cryst. Growth Des.*, 2017, **17**, 4458–4466.

20 J. Neu, E. A. Stone, J. A. Spies, G. Storch, A. S. Hatano, B. Q. Mercado, S. J. Miller and C. A. Schmuttenmaer, *J. Phys. Chem. Lett.*, 2019, **10**, 2624–2628.

21 K. A. Niessen, M. Xu, D. K. George, M. C. Chen, A. R. Ferré-D'amaré, E. H. Snell, V. Cody, J. Pace, M. Schmidt and A. G. Markelz, *Nat. Commun.*, 2019, **10**, 1–10.

22 S. P. Delaney and T. M. Korter, *J. Phys. Chem. A*, 2015, **119**, 3269–3276.

23 S. Pellizzeri, S. P. Delaney, T. M. Korter and J. Zubieta, *J. Phys. Chem. A*, 2013, **118**, 417–426.

24 M. T. Ruggiero, J. Sibik, J. A. Zeitler and T. M. Korter, *J. Phys. Chem. A*, 2016, **120**, 7490–7495.

25 N. R. Rexrode, J. Orien and M. D. King, *J. Phys. Chem. A*, 2019, **123**, 6937–6947.

26 M. T. Ruggiero, J. A. Zeitler and T. M. Korter, *Phys. Chem. Chem. Phys.*, 2017, **19**, 28502–28506.

27 H. Li, H.-M. Ye and Y. Yang, *Polym. Test.*, 2017, **57**, 52–57.

28 M. T. Ruggiero, J. J. Sutton, S. J. Fraser-Miller, A. J. Zaczek, T. M. Korter, K. C. Gordon and J. A. Zeitler, *Cryst. Growth Des.*, 2018, **18**, 6513–6520.

29 M. T. Ruggiero, *J. Infrared, Millimeter, Terahertz Waves*, 2020, **41**, 491–528.

30 Y. Noel, C. M. Zicovich-Wilson, B. Civalleri, P. D'Arco and R. Dovesi, *Phys. Rev. B: Condens. Matter Mater. Phys.*, 2002, **65**, 1–9.

31 M. D. King, W. D. Buchanan and T. M. Korter, *Phys. Chem. Chem. Phys.*, 2011, **13**, 4250.

32 T. R. Juliano, M. D. King and T. M. Korter, *IEEE Trans. Terahertz Sci. Technol.*, 2013, **3**, 281–287.

33 M. F. Peintinger, D. V. Oliveira and T. Bredow, *J. Comput. Chem.*, 2012, **34**, 451–459.

34 D. Vilela Oliveira, J. Laun, M. F. Peintinger and T. Bredow, *J. Comput. Chem.*, 2019, **40**, 2364–2376.

35 D. Sidler, M. Meuwly and P. Hamm, *J. Chem. Phys.*, 2018, **148**, 244504.

36 M. T. Ruggiero, J. Gooch, J. Zubieta and T. M. Korter, *J. Phys. Chem. A*, 2016, **120**, 939–947.

37 T. Kleine-Ostmann, R. Wilk, F. Rutz, M. Koch, H. Niemann, B. Güttler, K. Brandhorst and J. Grunenberg, *Chem. Phys. Chem.*, 2008, **9**, 544–547.

38 L. M. Lepodise, J. Horvat and R. A. Lewis, *J. Phys. Chem. A*, 2015, **119**, 270.

39 K. Ajito, Y. Ueno, J.-Y. Kim and T. Sumikama, *J. Am. Chem. Soc.*, 2018, **140**, 13793–13797.

40 M. Amalanathan, I. H. Joe and S. S. Prabhu, *J. Phys. Chem. A*, 2010, **114**, 13055–13064.

41 Y. Sun, X. Lu, P. Du, P. Xie and R. Ullah, *Spectrochim. Acta, Part A*, 2019, **209**, 70–77.

42 X. Yu, W. Fan, G. Wang, S. Lin, Z. Li, M. Liu, Y. Yang, X. Xin and Q. Jin, *Polyhedron*, 2019, **157**, 301–309.

43 Y. Liu, T. Zhou and J.-C. Cao, *Infrared Phys. Technol.*, 2019, **96**, 17–21.

44 P. S. Sindhu, D. Prasad, S. Peli, N. Mitra and P. Datta, *J. Mol. Struct.*, 2019, **1184**, 114–122.

45 Y. Wang, J. Xue, Q. Wang, S. Jin, Z. Zhang, Z. Hong and Y. Du, *Spectrochim. Acta, Part A*, 2019, **216**, 98–104.

46 Z. Zhang, Q. Cai, J. Xue, J. Qin, J. Liu, Y. Du, Z. Zhang, Q. Cai, J. Xue, J. Qin, J. Liu and Y. Du, *Pharmaceutics*, 2019, **11**, 56.

47 A. James and R. S. Swathi, *J. Phys. Chem. C*, 2019, **123**, 10544–10556.

48 Y. Wang, J. Xue, J. Qin, J. Liu and Y. Du, *Spectrochim. Acta, Part A*, 2019, **219**, 419–426.

49 Y. Zhao, Z. Li, J. Liu, C. Hu, H. Zhang, B. Qin and Y. Wu, *Spectrochim. Acta, Part A*, 2018, **189**, 528–534.

50 C. Guadarrama-Pérez, J. M. Martínez De, L. Hoz and P. B. Balbuena, *J. Phys. Chem. A*, 2010, **114**, 2284–2292.

51 J. Yang, S. Li, H. Zhao, B. Song, G. Zhang, J. Zhang, Y. Zhu and J. Han, *J. Phys. Chem. A*, 2014, **118**, 10927–10933.

52 J. Dash, S. Ray, K. Nallappan, V. Kaware, N. Basutkar, R. G. Gonnade, A. V. Ambade, K. Joshi and B. Pesala, *J. Phys. Chem. A*, 2015, **119**, 7991–7999.

53 P. B. Balbuena, W. Blocker, R. M. Dudek, F. A. Cabrales-Navarro and P. Hirunsit, *J. Phys. Chem. A*, 2008, **112**, 10210–10219.

54 D. S. Tikhonov, D. I. Sharapa, A. A. Otlyotov, P. M. Solyankin, A. N. Rykov, A. P. Shkurinov, O. E. Grikina and L. S. Khaikin, *J. Phys. Chem. A*, 2018, **122**, 1691–1701.

55 P. Guevara Level, H. Santos Silva, F. Spillebout, K. H. Michaelian, J. M. Shaw, I. Baraille, D. Bégué and B. Bégué, *J. Phys. Chem. A*, 2017, **121**, 7205–7218.

56 D. M. Mittleman, *J. Appl. Phys.*, 2017, **122**, 230901.

57 P. R. Smith, D. H. Auston and M. C. Nuss, *IEEE J. Quantum Electron.*, 1988, **24**, 255–260.

58 E. P. Parrott and J. A. Zeitler, *Appl. Spectrosc.*, 2015, **69**, 1–25.

59 X. C. Zhang, X. F. Ma, Y. Jin, T. M. Lu, E. P. Boden, P. D. Phelps, K. R. Stewart and C. P. Yakymyshyn, *Appl. Phys. Lett.*, 1992, **61**, 3080–3082.

60 A. Rice, Y. Jin, X. F. Ma, X. C. Zhang, D. Bliss, J. Larkin and M. Alexander, *Appl. Phys. Lett.*, 1994, **64**, 1324–1326.

61 Q. Wu, M. Litz and X. C. Zhang, *Appl. Phys. Lett.*, 1996, **68**, 2924–2926.

62 S. S. Dhillon, M. S. Vitiello, E. H. Linfield, A. G. Davies, M. C. Hoffmann, J. Booske, C. Paoloni, M. Gensch, P. Weightman, G. P. Williams, E. Castro-Camus, D. R. S. Cumming, F. Simoens, I. Escorcia-Carranza, J. Grant, S. Lucyszyn, M. Kuwata-Gonokami, K. Konishi, M. Koch, C. A. Schmuttenmaer, T. L. Cocker, R. Huber, A. G. Markelz, Z. D. Taylor, V. P. Wallace, J. A. Zeitler, J. Sibik, T. M. Korter, B. Ellison, S. Rea, P. Goldsmith, K. B. Cooper, R. Appleby, D. Pardo, P. G. Huggard, V. Krozer, H. Shams, M. Fice, C. Renaud, A. Seeds, A. Stöhr, M. Naftaly, N. Ridler, R. Clarke, J. E. Cunningham and M. B. Johnston, *J. Phys. D: Appl. Phys.*, 2017, **50**, 1–49.

This journal is © the Owner Societies 2021

Phys. Chem. Chem. Phys., 2021, **23**, 20038–20051 | **20049**

63 N. M. Burford and M. O. El-Shenawee, *Opt. Eng.*, 2017, **56**, 010901.

64 P. Y. Han, M. Tani, F. Pan and X.-C. Zhang, *Opt. Lett.*, 2000, **25**, 675.

65 F. D. J. Brunner, O.-P. Kwon, S.-J. Kwon, M. Jazbinšek, A. Schneider and P. Günter, *Opt. Express*, 2008, **16**, 16496.

66 Y.-S. Lee, T. Meade, V. Perlin, H. Winful, T. B. Norris and A. Galvanauskas, *Appl. Phys. Lett.*, 2000, **76**, 2505–2507.

67 P. U. Jepsen, C. Winnewisser, M. Schall, V. Schyja, S. R. Keiding and H. Helm, *Phys. Rev. E: Stat. Phys., Plasmas, Fluids, Relat. Interdiscip. Top.*, 1996, **53**, R3052–R3054.

68 M. Jazbinsek, U. Puc, A. Abina and A. Zidansek, *Appl. Sci.*, 2019, **9**, 882.

69 B. Clough, J. Dai and X. C. Zhang, *Mater. Today*, 2012, **15**, 50–58.

70 P. Dean, A. Valavanis, J. Keeley, K. Bertling, Y. L. Lim, R. Alhathlool, A. D. Burnett, L. H. Li, S. P. Khanna and D. Indjin, *et al.*, *J. Phys. D: Appl. Phys.*, 2014, **47**, 374008.

71 D. F. Swearer, S. Gottheim, J. G. Simmons, D. J. Phillips, M. J. Kale, M. J. McClain, P. Christopher, N. J. Halas and H. O. Everitt, *ACS Photonics*, 2018, **5**, 3097–3106.

72 M. van Exter, C. Fattinger and D. Grischkowsky, *Opt. Lett.*, 1989, **14**, 1128–1130.

73 B. J. Drouin, H. Gupta, S. Yu, C. E. Miller and H. S. Müller, *J. Chem. Phys.*, 2012, **137**, 024305.

74 O. Lakhmanskaya, M. Simpson, S. Murauer, M. Notzold, E. Endres, V. Kokoouline and R. Wester, *Phys. Rev. Lett.*, 2018, **120**, 253003.

75 C. M. Persson, M. Hajigholi, G. E. Hassel, A. O. H. Olofsson, J. H. Black, E. Herbst, H. S. P. Müller, J. Cernicharo, E. S. Wirström, M. Olberg, Å. Hjalmarson, D. C. Lis, H. M. Cuppen, M. Gerin and K. M. Menten, *Astron. Astrophys.*, 2014, **567**, A130.

76 H.-W. Hübers, H. Richter and M. Wienold, *J. Appl. Phys.*, 2019, **125**, 151401.

77 H.-W. Hübers, S. G. Pavlov, H. Richter, A. D. Semenov, L. Mahler, A. Tredicucci, H. E. Beere and D. A. Ritchie, *Appl. Phys. Lett.*, 2006, **89**, 061115.

78 M. C. Beard, G. M. Turner and C. A. Schmuttenmaer, *J. Appl. Phys.*, 2001, **90**, 5915–5923.

79 T. L. Cocker, L. V. Titova, S. Fourmaux, H. C. Bandulet, D. Brassard, J. C. Kieffer, M. A. El Khakani and F. A. Hegmann, *Appl. Phys. Lett.*, 2010, **97**, 221905.

80 K. Kushnir, Y. Qin, Y. Shen, G. Li, B. M. Fregoso, S. Tongay and L. V. Titova, *ACS Appl. Mater. Interfaces*, 2019, **11**, 5492–5498.

81 D. Zhao, H. Hu, R. Haselsberger, R. A. Marcus, M.-E. Michel-Beyerle, Y. M. Lam, J.-X. Zhu, C. Laovorakiat, M. C. Beard and E. E. M. Chia, *ACS Nano*, 2019, **13**, 8826–8835.

82 B. Guzelturk, R. A. Belisle, M. D. Smith, K. Bruening, R. Prasanna, Y. Yuan, V. Gopalan, C. J. Tassone, H. I. Karunadasa, M. D. McGehee and A. M. Lindenberg, *Adv. Mater.*, 2018, **30**, 1704737.

83 B. Pattengale, J. Neu, S. Ostresh, G. Hu, J. A. Spies, R. Okabe, G. W. Brudvig and C. A. Schmuttenmaer, *J. Am. Chem. Soc.*, 2019, **141**, 9793–9797.

84 J. A. Zeitler, P. F. Taday, D. A. Newnham, M. Pepper, K. C. Gordon and T. Rades, *J. Pharm. Pharmacol.*, 2007, **59**, 209–223.

85 S. Stranzinger, E. Faulhammer, J. Li, R. Dong, J. G. Khinast, J. A. Zeitler and D. Markl, *Powder Technol.*, 2019, **344**, 152–160.

86 J. F. Federici, B. Schulkin, F. Huang, D. Gary, R. Barat, F. Oliveira and D. Zimdars, *Semicond. Sci. Technol.*, 2005, **20**, S266–S280.

87 C. L. K. Dandolo and P. U. Jepsen, *J. Infrared, Millimeter, Terahertz Waves*, 2015, **37**, 198–208.

88 Y. Ghasempour, R. Shrestha, A. Charous, E. Knightly and D. M. Mittleman, *Nat. Commun.*, 2020, **11**, 1–6.

89 J. Sibik and J. A. Zeitler, *Philos. Mag.*, 2015, **96**, 842–853.

90 M. T. Ruggiero, M. Krynski, E. O. Kissi, J. Sibik, D. Markl, N. Y. Tan, D. Arslanov, W. van der Zande, B. Redlich and T. M. Korter, *et al.*, *Phys. Chem. Chem. Phys.*, 2017, **19**, 30039–30047.

91 J. A. Zeitler, P. F. Taday, K. C. Gordon, M. Pepper and T. Rades, *Chem. Phys. Chem.*, 2007, **8**, 1924–1927.

92 M. T. Ruggiero and T. M. Korter, *Phys. Chem. Chem. Phys.*, 2016, **18**, 5521–5528.

93 W. Zhang, Z. Song, M. T. Ruggiero and D. M. Mittleman, *J. Infrared, Millimeter, Terahertz Waves*, 2020, **41**, 1355–1365.

94 P. A. Banks, Z. Song and M. T. Ruggiero, *J. Infrared, Millimeter, Terahertz Waves*, 2020, **41**, 1–19.

95 X. Dai, S. Fan, Z. Qian, R. Wang, V. P. Wallace and Y. Sun, *Spectrochim. Acta, Part A*, 2020, **236**, 118330.

96 M. T. Ruggiero and J. A. Zeitler, *J. Phys. Chem. B*, 2016, **120**, 11733–11739.

97 Z. Zhang, J. Fang, Y. Bo, J. Xue, J. Liu, Z. Hong and Y. Du, *J. Mol. Struct.*, 2021, **1227**, 129547.

98 T. Chen, Q. Zhang, Z. Li, X. Yin and F. Hu, *Spectrochim. Acta, Part A*, 2018, **205**, 312–319.

99 T. Chen, Q. Zhang, Z. Li and F. Hu, *J. Lumin.*, 2020, **223**, 117198.

100 D. Tomerini and G. M. Day, in *Terahertz Spectroscopy and Imaging*, ed. K.E. Peiponen, J. A. Zeitler, and M. Kuwata-Gonokami, Springer, Berlin, Heidelberg, 2012, ch. 7, pp. 151–190.

101 Q. Chen, S. Jia, J. Qin, Y. Du and Z. Zhao, *J. Spectrosc.*, 2020, **2020**, 1–10.

102 X. Wu, L. Wang, Y. Peng, F. Wu, J. Cao, X. Chen, W. Wu, H. Yang, M. Xing, Y. Zhu, Y. Shi and S. Zhuang, *Analyst*, 2020, **145**, 3909–3915.

103 X. Wu, Y. Wang, J. Xue, J. Liu, J. Qin, Z. Hong and Y. Du, *Spectrochim. Acta, Part A*, 2020, **234**, 118265.

104 W. Zhang, Y. Yang, P. Suo, W. Zhao, J. Guo, Q. Lu, X. Lin, Z. Jin, L. Wang, G. Chen and F. Xiu, *ACS Omega*, 2020, **5**, 17266–17274.

105 H. Takeda, H. Yoshioka, H. Minamide, Y. Oki and C. Aadachi, *Opt. Commun.*, 2020, **476**, 126339.

106 F. Qu, L. Lin, C. Cai, B. Chu, Y. Wang, Y. He and P. Nie, *Food Chem.*, 2021, **334**, 127474.

107 R. Yang, X. Dong, F. Lin, Z. Huang, M. Manzo and H. Mao, *Polymers*, 2021, **23**, 1–13.

108 Q. Zhang, T. Chen, L. Ma, Z. Tang and L. Yu, *Chem. Phys. Lett.*, 2021, **767**, 138350.

109 Y. Bian, X. Zhang, Z. Zhu and B. Yang, *J. Mol. Struct.*, 2021, **1232**, 129952.

110 R. Dovesi, A. Erba, R. Orlando, C. M. Zicovich-Wilson, B. Civalleri, L. Maschio, M. Rérat, S. Casassa, J. Baima, S. Salustro and B. Kirtman, *WIREs Comput. Mol. Sci.*, 2018, **8**, e1360.

111 G. E. S. M. J. Frisch, G. W. Trucks, H. B. Schlegel, B. M. M. A. Robb, J. R. Cheeseman, G. Scalmani, V. Barone, H. P. H. G. A. Petersson, H. Nakatsuji, M. Caricato, X. Li, M. H. A. F. Izmaylov, J. Bloino, G. Zheng, J. L. Sonnenberg, T. N. M. Ehara, K. Toyota, R. Fukuda, J. Hasegawa, M. Ishida, J. Y. Honda, O. Kitao, H. Nakai, T. Vreven, J. A. Montgomery, E. B. J. E. Peralta, F. Ogliaro, M. Bearpark, J. J. Heyd, J. N. K. N. Kudin, V. N. Staroverov, T. Keith, R. Kobayashi, J. T. K. Raghavachari, A. Rendell, J. C. Burant, S. S. Iyengar, J. B. C. M. Cossi, N. Rega, J. M. Millam, M. Klene, J. E. Knox, R. E. S. V. Bakken, C. Adamo, J. Jaramillo, R. Gomperts, J. W. O. O. Yazyev, A. J. Austin, R. Cammi, C. Pomelli, G. A. V. R. L. Martin, K. Morokuma, V. G. Zakrzewski, A. D. D. P. Salvador, J. J. Dannenberg, S. Dapprich and D. J. F. O. Farkas, J. B. Foresman, J. V. Ortiz, J. Cioslowski, *Gaussian 09, Revision D.01*, 2013.

112 S. J. Dampf and T. M. Korter, *J. Infrared, Millimeter, Terahertz Waves*, 2020, **41**, 1284–1300.

113 A. D. Becke, *J. Chem. Phys.*, 1993, **98**, 4775.

114 S. Grimme, J. Antony, S. Ehrlich and H. Krieg, *J. Chem. Phys.*, 2010, **132**, 44115.

115 S. Grimme, S. Ehrlich and L. Goerigk, *J. Comput. Chem.*, 2011, **32**, 1456–1465.

116 F. Weigend and R. Ahlrichs, *Phys. Chem. Chem. Phys.*, 2005, **7**, 3297–3305.

117 A. Schäfer, H. Horn and R. Ahlrichs, *J. Chem. Phys.*, 1992, **97**, 2571–2577.

118 V. R. Thalladi, M. Nu and R. Boese, *J. Am. Chem. Soc.*, 2000, **122**, 9227–9236.

119 A. D. Becke, *J. Chem. Phys.*, 1993, **98**, 1372–1377.

120 C. Lee, E. Yang and R. G. Parr, *Phys. Rev. B: Condens. Matter Mater. Phys.*, 1988, **37**, 785–789.

121 M. D. King and T. M. Korter, *J. Phys. Chem. A*, 2010, **114**, 7127–7138.

122 E. P. J. Parrott, N. Y. Tan, R. Hu, J. A. Zeitler, B. Z. Tang and E. Pickwell-MacPherson, *Mater. Horiz.*, 2014, **1**, 251–258.

123 D. Allis, A. Fedor, T. Korter, J. Bjarnason and E. Brown, *Chem. Phys. Lett.*, 2007, **440**, 203–209.

124 S. Yamauchi, S. Hatakeyam, Y. Imai and M. Tonouchi, *Am. J. Anal. Chem.*, 2013, **4**, 756–762.

125 J. H. Smith, S. E. Dann, M. R. J. Elsegood, S. H. Dale and C. G. Blatchford, *Acta Crystallogr., Sect. E: Struct. Rep. Online*, 2005, **61**, 2499–2501.

126 S. Garnier, S. Petit and G. Coquerel, *J. Therm. Anal. Calorim.*, 2002, **68**, 489–502.

This journal is © the Owner Societies 2021

Phys. Chem. Chem. Phys., 2021, **23**, 20038–20051 | **20051**